Linearized Piecewise Affine in Control and States Hydraulic System: Modeling and Identification

Philipp Pasolli
University of Agder (UiA)
Faculty of Engineering and Science
Post box 422, 4604-Kristiansand, Norway
philipp.pasolli@uia.no

Michael Ruderman
University of Agder (UiA)
Faculty of Engineering and Science
Post box 422, 4604-Kristiansand, Norway
michael.ruderman@uia.no

***Abstract*—In this paper, the modeling and identification of a nonlinear actuated hydraulic system is addressed. The full-order model is first reduced in relation to the load pressure and flow dynamics and, based thereupon, linearized over the entire operational state-space. The dynamics of the proportional control valve is identified, analyzed, and intentionally excluded from the reduced model, due to a unity gain behavior in the frequency range of interest. The input saturation and dead-zone nonlinearities are considered while the latter is identified to be close to 10% of the valve opening. The mechanical part includes the Stribeck friction detected and estimated from the experiments. The linearization is performed in multiple steps, for the most pronounced terms of nonlinear system dynamics. Out of this follows a linearized piecewise affine in the control and state model in a state-dependent matrix form. A series of measurements were performed on the designed and implemented experimental setup, while identifying uncertain parameters of the system, in addition to those obtained from the technical data and characteristics of components. The models behavior are compared with experimental measurements and discussed.**

I. Introduction

When it comes to applications demanding high power in relatively small form factor, hydraulic systems and actuators [1], [2] still remain the first choice. However, hydraulic systems are also known for their nonlinear behavior making it challenging for operation in the force control [3] and motion control [4] modes, and a hybrid combination of both e.g. [5]. Correspondingly, the control design, tuning, and evaluation require an advanced system knowledge and associated modeling and identification. One goal can be to create simplified models, mostly linearized around some operation points, e.g. [3], [6]–[9]. On the other hand, more detailed modeling of the single hydraulic components, like a unified one proposed for proportional valves in [10], requires yet an explicit knowledge of the mechanical assemblies and, mostly, an accurate identification of the internal states and characteristics, that is generally not feasible under regular operation conditions. Nevertheless, multiple system- and control-oriented studies considered extended, to say full-order, system dynamics while incorporating the most pronounced nonlinearities nested within electrical, hydraulic, and mechanical subsystems of a hydraulic drive as a whole, see e.g. [4], [5], [11], [12]. A comparison between a full-order model and its reduced counterpart, including local linearization, has been recently shown in [13]. At the same time, a hybrid system consideration, and piecewise affine as one of particularly handy subclasses of that, appears promising also for hydraulic systems over a large operation range. For more advanced studies on identification techniques for the hybrid systems we refer to [14]–[16].

In this paper, we assume the main sources of nonlinearities during the system modeling and introduce, based thereupon, a linearized piecewise affine in the control and states model of an actuated hydraulic cylinder supplied via a controlled servo valve. Recall that a general class of nonlinear systems affine in the control assumes a vector field state-space notation

$$\dot{\mathbf{x}} = f(\mathbf{x}) + g(\mathbf{x})u,$$

cf. [17], while the affine (linear with offset) state dynamics [18] requires from us inclusion of an additional constant vector term. We rely on a linearized piecewise affine formulation of a state-space model, while believing it can yield further advantages for the analysis and control design, also in spirit of the hybrid control systems [19], [20] and their computational, to say formal, verification [21]. It is worth noting that even without affine state dynamics, the affine (only in control) linear parameter-varying models are challenging as for structural identifiability and parameterizations [22]. For particular dynamic systems, i.e. valve-controlled hydraulic drives, we propose an approach for linearized piecewise affine modeling.

The rest of the paper is organized as follows. The paper starts with the full-order model in Section II, while taking the necessary steps of the model reduction in Section III. The state-space model, affine in both control and states, is formulated in Section IV, including the piecewise affine linearization at various points. In Section V the experimental setup is described. The parameter identification is shown in Section VI, and an evaluating comparison between the different models and data from the motion experiments is provided in Section VII. Lastly a brief summary is given in Section VIII.

II. Full-order model

Below, the full-order model of the system is first described. We distinguish between modeling the valves characteristics, orifice equations, continuity equations, and mechanical sub-model of the hydraulic cylinder. Note that the full-order model

Preprint of the manuscript accepted to IEEE 44th Annual Conference of Industrial Electronics Society (IECON2018)

can be directly derived from the basics on hydraulic systems to be found in the standard literature e.g. [1], [2].

A. Servo valve approximation

The controlled servo valve can be approximated by a second-order dynamic system, with the spools' position ν as output, so that the input-output transfer function is

$$G(s) = \frac{\nu(s)}{u(s)} = \frac{\omega_0^2}{s^2 + 2\zeta\omega_0 s + \omega_0^2}. \tag{1}$$

Here, ζ is the damping coefficient and ω_0 is the natural frequency of the closed-loop dynamics. The external control signal is denoted by u. Values for ω_0 and ζ are subject to variations, depending on the input amplitude $|u|$, as pointed out in the FRF (frequency response function) of the data sheets provided by the valves' manufacturer. According to the technical data sheet, the servo valve we consider has a 10% overlap in the spool-orifice area, thus, introducing a dead-zone. Furthermore, the valve is inherently limited in how far it can open, therefore being subject to an additional saturation. The combination of dead-zone and saturation nonlinearities can be described as in [13] by

$$h(\nu) = \begin{cases} \alpha \cdot \operatorname{sign}(\nu), & \text{if } |\nu| \geq \alpha + \beta, \\ 0, & \text{if } |\nu| < \beta, \\ \nu - \beta \cdot \operatorname{sign}(\nu), & \text{otherwise}, \end{cases} \tag{2}$$

where the parameters α and β are the valve saturation and dead-zone width, respectively. As the dead-zone is of a constructive, i.e. mechanical, nature, its transfer characteristic has to be placed in series with the servo valve model. Several previous works [3]–[5], [11], [23] neglected, or only partially accounted for, the mentioned combination of the saturation and dead-zone. Both can, however, have a non-negligible impact on the overall system dynamics. At the end, the entire sub-model of the controlled servo valve is described by

$$\ddot{\nu} + 2\zeta\omega_0\dot{\nu} + \omega_0^2\nu = \omega_0^2 u, \tag{3}$$

$$z = h(\nu), \tag{4}$$

while z is an internal state representing the orifice opening.

B. Orifice and continuity equations

The orifice equations describe the hydraulic flow Q through the valve, respectively in regards of the pressure drop, as

$$Q_A = \begin{cases} zK\sqrt{P_S - P_A} & \text{for } z > 0 \\ zK\sqrt{P_A - P_T} & \text{for } z < 0 \\ 0 & \text{otherwise}, \end{cases} \tag{5}$$

$$Q_B = \begin{cases} zK\sqrt{P_B - P_T} & \text{for } z > 0 \\ zK\sqrt{P_S - P_B} & \text{for } z < 0 \\ 0 & \text{otherwise}, \end{cases} \tag{6}$$

and that for both ports, correspondingly load connections of the hydraulic circuit. The pressure indices A, B, T, S refer to the servo valves' inlets and outlets, i.e. to the A and B connection ports, tank, and pressure supply respectively. Well-known, K represents the valves' flow coefficient

$$K = c_d\omega\sqrt{\frac{2}{\rho}}, \tag{7}$$

with the constructive valves' parameters, in addition to the oil density ρ. At the same time, from the technical data sheet, one can assume a characteristic relationship

$$Q = Q_n\sqrt{\frac{\Delta p}{p_n}}, \tag{8}$$

where Δp is the pressure drop across the valve, and Q_n, p_n are the nominal flow and pressure drop, describing the valves behavior in a fully open state. By rearranging (8), it can be seen that $Q_n(\sqrt{p_n})^{-1}$ is equivalent to the flow coefficient K, that allows omitting the identification of ω, c_d and ρ parameters. This way, the valves' flow coefficient is determined from the nominal pressure drop and flow characteristics given by the technical data sheet.

Knowing the flow through the valve, the pressure drop can be calculated directly, via the continuity equations

$$\begin{aligned} \dot{P}_B = &\quad \frac{E}{V_B + A_B(l - x)} \cdot \left(Q_B + A_B\dot{x} + C_L\left(P_A - P_B\right)\right) \\ \dot{P}_A = &\quad \frac{E}{V_A + A_A x} \cdot \left(Q_A - A_A\dot{x} + C_L\left(P_B - P_A\right)\right), \end{aligned} \tag{9}$$

where $V_{A/B}$ is the volume of the hydraulic oil in the tubing between the valve and both A/B-chambers of the cylinder, while $A_A x$ and $A_B(l - x)$ are the operational volumes of cylinder. Note that the total (maximal) stroke l provides mechanical constraints for the piston motion, so that $0 \leq x \leq l$, while x is the relative cylinders' rod position. E is the bulk modulus and C_L is an internal leakage coefficient. The latter characterizes the pressure drop across the membrane which is separating both cylinder chambers.

C. Mechanical sub-model of cylinder

The cylinder dynamics is modeled as a second-order system with one DOF (degree of freedom) described by

$$m\ddot{x} = P_A A_A - P_B A_B - f(\dot{x}) - F_L. \tag{10}$$

The total mass under actuation is m, and $f(\dot{x})$ constitutes the entire friction force acting against the rods' motion. F_L is the load force applied externally, which can be measured by a force sensor, cf. further Fig. 4. The lumped mass is calculated from the data sheets of all moving components in the assembly, while the cross sections of both chambers $A_A \neq A_B$ are taken from the available technical drawings. The nonlinear velocity-dependent Stribeck friction model, see e.g. [24], is taken for $f(\dot{x})$. To avoid a sign-related discontinuity, a hyperbolic tangent has been assumed, cf. [13], therefore resulting in a Stribeck type friction model

$$f(\dot{x}) = \tanh(\gamma\dot{x})\Big(F_c + (F_s - F_c)\exp\Big(-\Big|\frac{\dot{x}}{\chi}\Big|^{\delta}\Big)\Big) + \sigma\dot{x}. \tag{11}$$

The Coulomb friction coefficient is stated as $F_c > 0$, stiction coefficient as $F_s > F_c$, the linear viscous friction coefficient as $\sigma > 0$. Two Stribeck shape parameters are $\delta \neq 0$ and $\chi > 0$. The parameter γ scales the smoothness of zero crossing transition, until its saturated value $\to \pm 1$ approaches the velocity-dependent sign. Note that more complex dynamic

friction behavior [25] is purposefully not considered, since for the largely damped and relatively slow hydraulic systems the modeling (11) can yield as fairly sufficient, cf. [3], [23].

III. Model Reduction

From the available FRFs of the servo valve, shown further in Section VI, as identified for 10%, 25% and 90% opening, one can neglect the closed-loop dynamics in the lower frequency range of interest. Therefore, a unity gain and an acceptably low phase lag can be considered, leading to the replacement of (3) by $u = \nu$. Note that a hydraulic cylinder is to be operated clearly below 10Hz frequency, cf. Figs. 5a, 5b, so that the above assumption is valid for modeling reduction. Note that (2) remains an input nonlinearity to be accounted for.

For the further model reduction, cf. [13] for details, a load-dependent pressure $P_L = P_A - P_B$ is introduced and $|Q_A| = |Q_B|$ is assumed for a closed hydraulic circuit. Therefore, the orifice equations (5), (6) are combined into

$$Q_L = zK\sqrt{\frac{1}{2}\left(P_S - \mathrm{sign}(z)P_L\right)}, \tag{12}$$

while

$$P_A = \frac{P_S + P_L}{2}, \quad P_B = \frac{P_S - P_L}{2}. \tag{13}$$

Following the above aggregation, the continuity eqs. (9) can be also combined into one:

$$\dot{P}_L = \frac{4E}{V_t}\left(Q_L - \bar{A}\dot{x} - C_L P_L\right). \tag{14}$$

In (14), $V_t = V_A + V_B$ represents the total actuator volume, and $\bar{A} = 0.5(A_B + A_A)$ is the averaged piston area. The latter will inherently lead to a certain model-reduction error once the piston has a single rod, thus yielding an asymmetric cylinder. Incorporating both above reduced equations into the cylinder dynamics (10) results in

$$m\ddot{x} = P_L\bar{A} - f(\dot{x}) - F_L. \tag{15}$$

IV. Nonlinear System Affine in Control and States

In order to model the system dynamics in a piecewise affine state-space formulation, several linerization steps are required.

Obviously, the combined dead-zone and saturation nonlinearity (2) can be described by

$$z = k_g \cdot u + d_g, \tag{16}$$

that partitions the total input range into the adjoining cells, indexed by g while $g = 1, \ldots, 5$.

For linearizing the orifice equation, the partial derivatives are first taken with respect to both variables z and P_L, thus resulting in two linearized parameters $\hat{C}_q$ and $\hat{C}_{qp}$. These, multiplied with the orifice opening and load pressure states respectively, yield the total load flow rate as

$$\hat{Q}_L = \hat{C}_q z - \hat{C}_{qp} P_L, \tag{17}$$

and that for a chosen working point $(\hat{z}, \hat{P}_L)$. Both terms of linearization can be computed as

$$\hat{C}_q = \left.\frac{\partial Q_L}{\partial z}\right|_{\hat{P}_L} = K\sqrt{0.5\left(P_S - \mathrm{sign}(z)\hat{P}_L\right)}, \tag{18}$$

$$\hat{C}_{qp} = \left.\frac{\partial Q_L}{\partial P_L}\right|_{\hat{z}} = \frac{\hat{z}K\mathrm{sign}(\hat{z})}{4\sqrt{0.5\left(P_S - \mathrm{sign}(\hat{z})P_L\right)}}. \tag{19}$$

One can recognize that, in order to capture the whole operation space, a piecewise affine mapping is required. That results in the state-dependent coefficients

$$C_q(P_L) = k_o P_L + d_o, \tag{20}$$

$$C_{qp}(P_L, z) = (k_n P_L + d_n)\, z. \tag{21}$$

Here again, the subscripts o and n represent the indices of the cells within state-space; k and d are the corresponding constants that parameterize the total piecewise affine model. Figure 1 shows $\hat{C}_q$ as well as its linearization C_q.

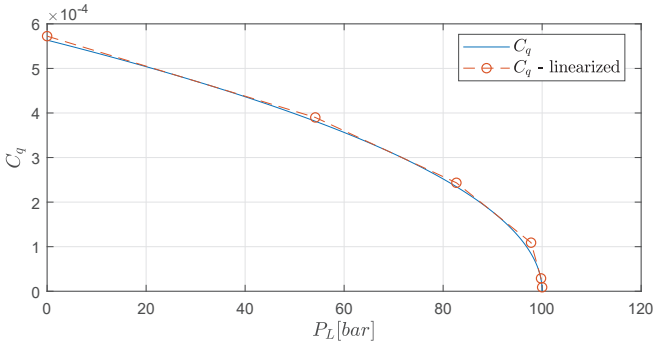

Fig. 1: $\hat{C}_q$ coefficient and its linearization

For $\hat{C}_{qp}$, the characteristic curves are shown in Fig. 2, together with linearization, for several representative values of z. Note that here the linearization was performed for a fully opened valve state, i.e. $z = 1$. The characteristic curves for $z < 1$ are then scaled down by multiplication with $\hat{z}$, according to (19). Note, that the linearized model does not take the supply pressure into account. Therefore the linearization process has to be performed for the intended supply pressure

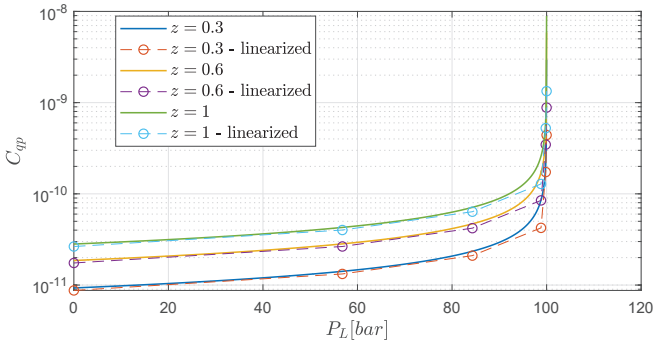

Fig. 2: $\hat{C}_{qp}$ coefficient and its linearization

and, consequently, the k and d values have to be recalculated once the supply pressure changes. By substituting (20) and (21) into (17), one can easily obtain the total orifice equation with the piecewise affine, yet state-dependent, coefficients.

In a similar way, the Stribeck friction model (11) is piecewise linearized as well, that results in

$$f(\dot{x}) = k_w \cdot \dot{x} + d_w, \tag{22}$$

while w in the cells index in the $\dot{x}$-space, and k and d are the corresponding constants.

When merging the above equations into the state dynamics (14), (15) one obtains the overall model in the following form

$$\dot{\mathbf{x}} = \mathbf{A(x)x} + \mathbf{b(x)}u + \mathbf{f}, \tag{23}$$
$$y = \mathbf{c}^T\mathbf{x}, \tag{24}$$

with the state vector $\mathbf{x} = [P_L, \dot{x}]^T$. That one incorporates the state-dependent system matrix $\mathbf{A}$, input coupling vector $\mathbf{b}$, and affine vector term $\mathbf{f}$. Note that since the cylinder stroke is not directly affecting the system dynamics, the total order is reduced by one. Obviously, one free integrator can be always connected in series with the system output (24), as it is done further for the model evaluation in Section VII, as long as no velocity measurement is provided. The modeling matrices, correspondingly vectors, are given by

$$\mathbf{A} = \begin{pmatrix} \frac{4Ed_g}{V_t}\left(k_o + k_n P_L + d_n - \frac{C_L}{d_g}\right) & -\frac{4E\bar{A}}{V_t} \\ \frac{\bar{A}}{m} & -\frac{k_w}{m} \end{pmatrix} \tag{25}$$

$$\mathbf{b} = \begin{pmatrix} \frac{4Ek_g P_L}{V_t}\left(k_o + \frac{d_o}{P_L} + k_n P_L + d_n\right) \\ 0 \end{pmatrix} \tag{26}$$

$$\mathbf{f} = \begin{pmatrix} \frac{4Ed_o d_g}{V_t} \\ -\frac{d_w + F_L}{m} \end{pmatrix} \tag{27}$$

$$\mathbf{c}^T = \begin{pmatrix} 0 & 1 \end{pmatrix} \tag{28}$$

V. Experimental Setup

The hydraulic system under investigation is shown in Fig. 3 (laboratory view). The schematic representation of the decoupled right-hand side cylinder is drawn in Fig. 4, where the sensing interfaces are indicated by ⊘. The system consists of a single rod, double-acting cylinders of type [26], with a linear force sensor [27] attached, that is measuring the respective load from the perspective of each cylinder. The cylinder under consideration is actuated via a 4/3 servo valve [28], attached to a hydraulic pump, with a maximum supply pressure of 350bar[1] and maximum flow rate of 120l/min. The pressures in both chambers of the cylinder are measured by the sensors [29]. Further, a linear potentiometer [30] is installed to track the

[1]Note that the pressure is denoted in bar, as conventionally for hydraulics, while standard SI units, i.e. Pa, are used for all calculations made

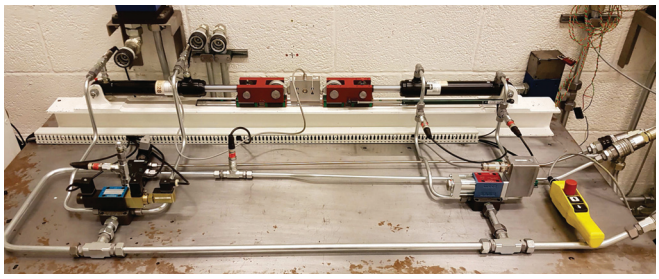

Fig. 3: Experimental hydraulic setup (laboratory view)

cylinders' rod position. The servo valve also includes a sensor for the spool position monitoring. As the real-time control interface between the development computer and experimental setup, the Speedgoat platform, baseline model S [31], with the IO183 and IO397 interface cards is used. This hardware

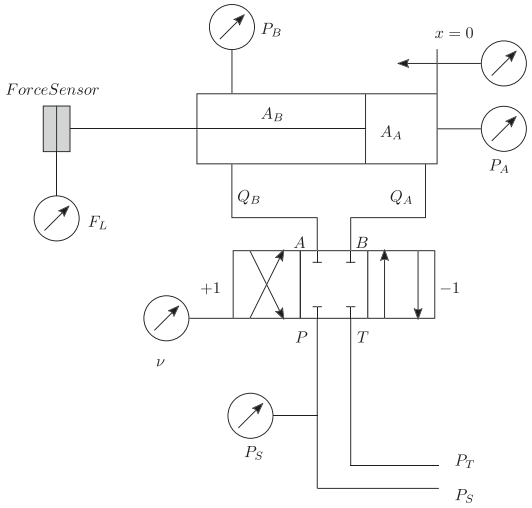

Fig. 4: Schematic representation of experimental setup

allows for a sampling rate of 2kHz. Furthermore, it supports 8 single-ended or 4 differential analogue input and 4 single ended output channels with a 16bit A/D and D/A converter each, as well as analog input voltages of ± 10V and output voltages of $0-5$V, with a maximum output current of 5mA on IO183. On IO387, 4 single-ended or 4 differential analogue input and 4 single ended output channels with a 16bit A/D and D/A converter each, as well as a analog input voltages of ± 10.24V and output voltages of ± 10V with a maximum output current of 5mA are available. An emergency break circuit was designed and implemented, switching all valves into a system pressure relieving, that means a 'no-motion' correspondingly 'no-force', configuration. The instrumented components are listed in Table I.

VI. Parameter Identification

In this section, the single identification steps for determining the unknown, correspondingly uncertain, system parameters are described. All experimental measurements, described below, were performed with a sampling frequency of 2kHz.

TABLE I: Installed components of experimental system

Description	Model number
Moog servo valve	D633 R16KD1M0NSM2
Cylinder	CD25-40 25x200-SS-HC-SSN-NNN
Danfoss P-sensor	MBS 1250 063G1229
Celesco linear-pot.	CLP-250
HBM Force sensor	1-S9M/50kN-1

A. Servo valve

In order to evaluate FRFs of the controlled servo valve, mentioned before, measurements were made to identify closed-loop frequency characteristics. Referring to (1), identification of the ω_0 and ζ parameters is required. To approach the nominal FRF characteristics, available from the data sheets, three different levels of the valve opening, 10%, 25% and 90%, are assumed, i.e. corresponding to the input magnitude $|u|$. For FRF measurements, sinusoidal signals were used, with frequencies starting from 2Hz and going up to 50Hz for 90% opening, and up to 100Hz for the rest. The equidistant

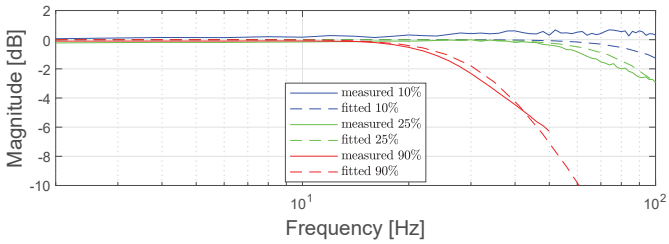

(a) Magnitude of the servo valve with different opening references

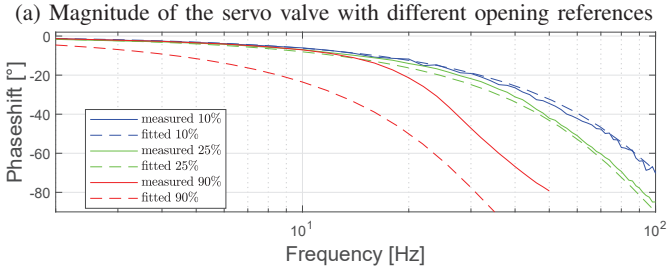

(b) Phase of the servo valve with different opening references

Fig. 5: Measured FRFs versus linear model fit

frequency interval is taken to be 2Hz. During the signal analysis the measured spool position was fitted over 4 periods with a sinusoidal curve for calculating, based thereupon, the magnitude and phase for each frequency measurement. The measurements and the fitted models are shown in Figs. 5a and 5b, while the determined model parameters are listed in Table II. The plots show that for 10% and 25% valve opening, the

TABLE II: Servo valve second-order model parameters

Valve opening [%]	$\omega_0\ [rad\,s^{-1}]$	ζ
10	816.8	0.7
25	628.3	0.7
90	220	0.7

model and the measurements are close to each other, while at 90% the parameters are adjusted to better fit the magnitude, to be inline with approximation from Section IV, while the phase response shows a stronger divergence.

B. Dead-zone

Measurements were performed to test the extend of the dead-zone in either direction from the middle (zero) position. For $u > 0$ the cylinders' initial position was fully retracted, while for $u < 0$ fully extended. The constant input signals were applied starting from 1% to 20% valve opening, and that in 0.5% steps. During the signal processing the cylinders' position signal was fitted with a linear function using the least squares method, revealing the slope and, therefore, constant velocity estimate of the rod $\hat{\dot{x}}$, shown in Fig. 6. Note that

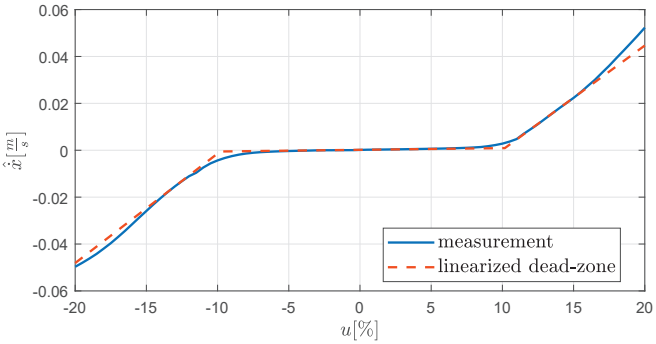

Fig. 6: Experimental test of the dead-zone and linearization

under these experimental conditions, a quasi-static behavior can be assumed, so that the appearance of non-zero velocity is directly associated with boundaries of the dead-zone. The plot shows a dead-band of around 10%, yet we still observe a very slow (rather creeping) cylinder motion also within the dead-band. Therefore, an ideal assumption of a fully locking dead-zone (2), is here not fully justified and a flat slope should be assumed for $|\nu| < \beta$, corresponding $k_g > 0$ in (16).

C. Stribeck friction

For positive u values, the rods' initial position is fully retracted, and fully extended for negative u values. Constant input signals, starting from 5% in 1% intervals up to 50%, were sent to the valve, while a constant counteracting force, produced by the second cylinder, was applied. Since the a constant valve opening is expected to generate a constant relative velocity at steady-state, and the full cylinder stroke was driven for all input values, the normed drive time is taken for the sake of comparison. The driven cylinder position over the normed time is shown in Fig. 7 for all measurements, and that for both directions. On the contrary to the full-order model, all measurements do not reveal an expected linear slope that corresponds to constant relative velocities. At the same time, a fairly good match of all curves and their mirroring symmetry for both directions point on some rather systematic behavior, which is obviously not captured even by the full-order model. A detailed analysis of this by-effect is, however,

out of the focus of this paper and builds an outlook for future works. For obtaining a reasonable estimate of relative velocities from the recorded experiments a least-squares fit of linear function (i.e. slope) has been made for all curves shown in Fig. 7. This yields a corresponding set of bidirectional

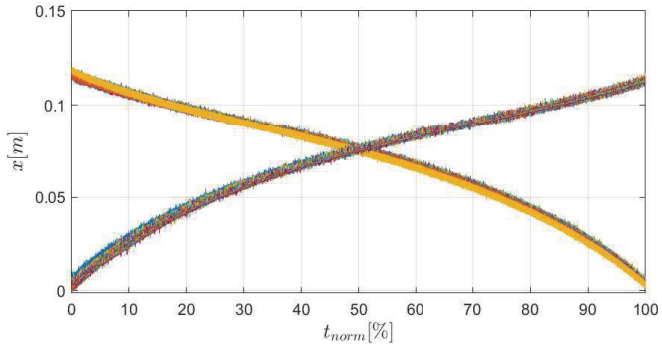

Fig. 7: Cylinder position measurements over normed time for all Stribeck curve measurements, 46 measurements for retracting and 45 measurements for extending motion

relative velocities, and that with the same extend of residual errors for the assumed linear slope. When calculating the friction force, the initial samples of each measurement show a transient, and that on both pressure sensors and force sensor. However, it has no apparent affect on the velocity of cylinder, as can be seen from Fig. 7. Therefore, only the steady-state part of each measurement was used for averaging P_B, P_A and F_L, thus allowing for calculating the cylinder forces according to (10). The obtained velocity-force data was used

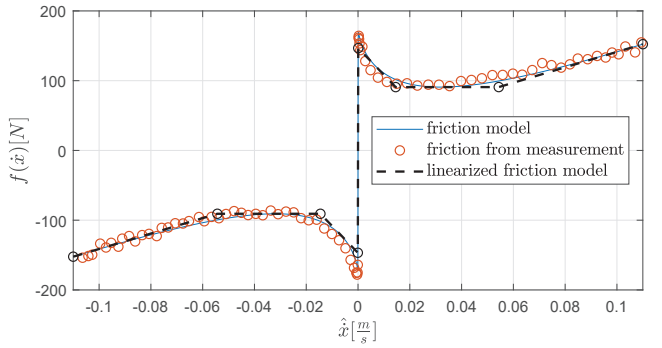

Fig. 8: Measured data points and fitted Stribeck model

to fit the Stribeck parameters, according to (11), by using the standard nonlinear least-squares method. During the following linearization, the curve was split into seven segments, four from which are representing the purely viscous and Coulomb friction contributions for both directions. The fitted Stribeck model and its piecewise linearization are shown together with the measured data in Fig. 8.

VII. Model Evaluation

Simulations were performed for all three models and compared with the corresponding measurements. As input a sinusoidal signal with frequencies of $f = [1, 2, 3]$Hz and amplitudes corresponding to the valve opening of $u = [20, 40, 60]\%$ were used. From the signals monitoring it was obvious that the supply pressure was varying from the 100bar set value during the drive, despite being connected to an oversized hydraulic power unit, cf. Fig. 9. Therefore, the measured pressure was used as the supply pressure input signal for the simulation. Plots of the 'corner' configurations, relating

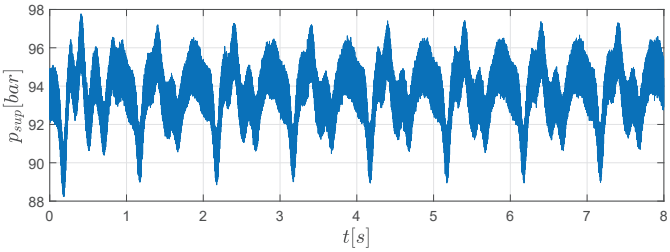

(a) 20% valve opening amplitude and frequency of 1Hz

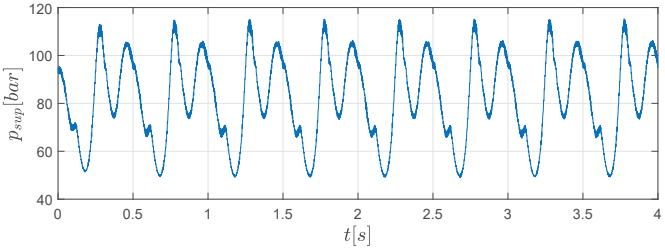

(b) 60% valve opening amplitude and frequency of 2Hz

Fig. 9: Measured supply pressure at sinusoidal input

to amplitude and frequency, are shown in Figs. 10, 11, 12 and 13. Initial conditions for pressures and cylinder position for the simulation were taken from the measurements at the start of the next full period once the steady-state condition can be observed. Also, starting from that point all initial values of the simulation were taken over from the available measurements. All identified, correspondingly computed, system parameters are given in Table III, while the corresponding linearization parameters are listed in Tables IV, V, VI, VII, VIII, IX. The linearization parameters for C_q and C_{qp}, listed in the tables, are each with four values, shown as an ordered set, with the order corresponding to four simulations presented. The experimental signals were processed using a moving average function, smoothing them for a better visual comparison.

From the results we can see a qualitatively similar behavior for all three models. The full-order model, equally as the measurements, shows an overall positive slope due to different cross sections of the piston, i.e. asymmetric cylinder. Furthermore, it can be seen that the qualitative response of the simulation and the measurement are fairly close. From Figs. 10, 12 one can recognize that at lower valve opening, i.e. at lower relative velocities, the measured displacement amplitude differs stronger comparing to the models. One of the possible reasons lies in a not fully linear displacement map at constant valve opening, correspondingly flow, cf. Fig. 7, and related identification of model parameters.

For the linearized model we observe a slightly drifting behavior. As mentioned in section IV, the linearization parameters for this model have to be recalculated if the supply pressure changes. For the shown simulation, an average supply pressure was calculated and used for calculation of the linearization parameters. An attempt of on-line recalculating the linearization parameters at the time-varying supply pressure fails due to an exponential increase in simulation time. The reduced model shows no drift in the graphs, in accord with the assumption that both sides piston areas are equal. Here the average supply pressure, the same as for the linearized model, was used to have a better comparison between the reduced and linearized model.

From comparison of the plots it can be said, that the cylinder motion predicted by the full-order model is best in accord with the measurements, especially in view of the relative displacement which has a free integrator behavior. Furthermore it can be noted, that there are almost no differences between the linearized and reduced order model besides a slight drifting motion of the linearized model due to the afore mentioned cell segmentation.

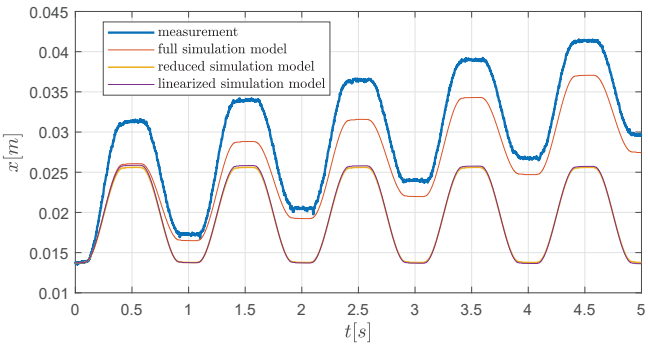

Fig. 10: Measurement and simulation for sinusoidal input with 20% valve opening and 1Hz frequency

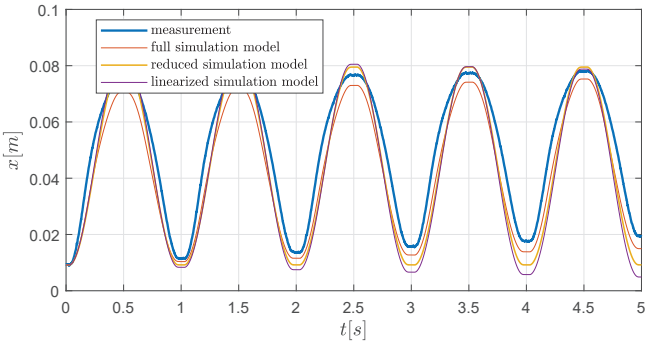

Fig. 11: Measurement and simulation for sinusoidal input with 60% valve opening and 1Hz frequency

VIII. Summary

Modeling of a hydraulic drive system was performed, including the full-order, reduced, and linearized models. Furthermore, the nonlinearities in the reduced model were located and linearized over the whole operational state-space, therefore resulting in a state-dependent matrix form affine in the control

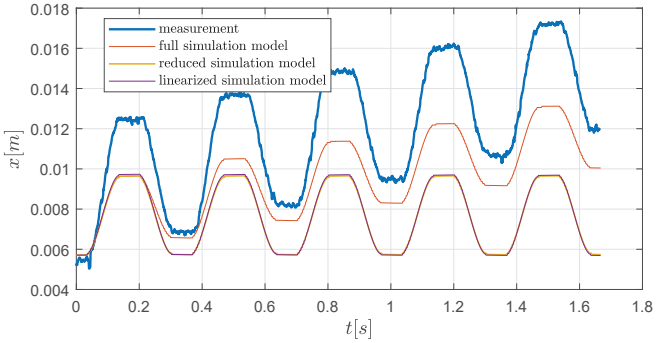

Fig. 12: Measurement and simulation for sinusoidal input with 20% valve opening and 3Hz frequency

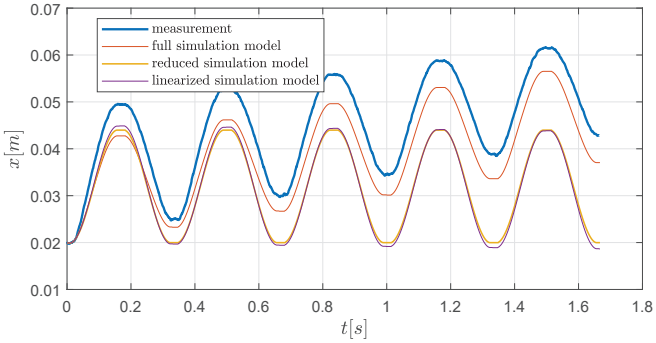

Fig. 13: Measurement and simulation for sinusoidal input with 60% valve opening and 3Hz frequency

TABLE III: Simulation Parameters

Param.	Value	Unit
m	1.394	kg
A_A	$1.3e^{-3}$	m^3
A_B	$0.76e^{-3}$	m^3
K	$0.252e^{-6}$	$\frac{m^3}{s\sqrt{Pa}}$
E	10^9	Pa

Param.	Value	Unit
P_T	0	Pa
V_A	0.7	m^3
V_B	0.7	m^3
F_L	0	N
C_L	0	$1/s$
l	0.2	m

TABLE IV: Values for linearized dead-zone and saturation

Cell	k_g	d_g
I	0	-1
II	1	0.1
III	0.04	0
IV	1	-0.1
V	0	1

TABLE V: Values for linearized Stribeck friction

Cell	k_w	d_w
I	1105	-30.7
II	-0.254	-90.8
III	-3867	-147
IV	$1.833e^3$	0
IV	-3867	147
IV	-0.819	90.7
IV	1105	30.7

TABLE VI: Values for k_o for linearized C_q

Cell	k_o
I	$[-0.034e^{-9}, -0.038e^{-9}, -0.035e^{-9}, -0.037e^{-9}]$
II	$[-0.053e^{-9}, -0.058e^{-9}, -0.053e^{-9}, -0.056e^{-9}]$
III	$[-0.092e^{-9}, -0.100e^{-9}, -0.092e^{-9}, -0.097e^{-9}]$
IV	$[-0.412e^{-9}, -0.447e^{-9}, -0.411e^{-9}, -0.435e^{-9}]$
V	$[-0.920e^{-9}, -0.998e^{-9}, -0.919e^{-9}, -0.972e^{-9}]$

TABLE VII: Values for d_o for linearized C_q

Cell	d_o
I	$[0.554e^{-3}, 0.510e^{-3}, 0.554e^{-3}, 0.525e^{-3}]$
II	$[0.647e^{-3}, 0.597e^{-3}, 0.648e^{-3}, 0.613e^{-3}]$
III	$[0.949e^{-3}, 0.874e^{-3}, 0.950e^{-3}, 0.899e^{-3}]$
IV	$[0.388e^{-3}, 3.573e^{-3}, 3.882e^{-3}, 3.671e^{-3}]$
V	$[8.632e^{-3}, 7.957e^{-3}, 8.646e^{-3}, 8.177e^{-3}]$

TABLE VIII: Values for k_n for linearized C_qp

Cell	k_o
I	$[0.027e^{-15}, 0.034e^{-15}, 0.026e^{-15}, 0.031e^{-15}]$
II	$[0.095e^{-15}, 0.121e^{-15}, 0.094e^{-15}, 0.111e^{-15}]$
III	$[0.491e^{-15}, 0.627e^{-15}, 0.489e^{-15}, 0.578e^{-15}]$
IV	$[43.93e^{-15}, 56.09e^{-15}, 43.71e^{-15}, 51.68e^{-15}]$
V	$[491.1e^{-15}, 627.1e^{-15}, 488.8e^{-15}, 577.8e^{-15}]$

TABLE IX: Values for d_n for linearized C_qp

Cell	d_o
I	$[\ 0.027e^{-9}, 0.030e^{-9}, 0.027e^{-9}, 0.029e^{-9}]$
II	$[-0.009e^{-9}, -0.009e^{-9}, -0.009e^{-9}, -0.009e^{-9}]$
III	$[-0.322e^{-9}, -0.349e^{-9}, -0.321e^{-9}, -0.340e^{-9}]$
IV	$[-40.54e^{-9}, -43.98e^{-9}, -40.48e^{-9}, -42.80e^{-9}]$
V	$[-458.8e^{-9}, -497.7e^{-9}, -458.1e^{-9}, -484.3e^{-9}]$

and states. The experimental hydraulic system was designed, constructed and instrumented, while incorporating a standard single-rod hydraulic cylinder operated via the controlled servo valve. Measurements were performed for analyzing the system dynamics and identifying the free parameters, otherwise weakly known from the technical data. These included FRFs of the valve closed-loop, the dead-zone and the nonlinear Stribeck-type friction. Simulations of all three models were exposed opposite to each other and compared with a set of measurements at different amplitudes and frequencies. Observed deviations were analyzed and discussed concerning the inherent sources and implications for modeling.

ACKNOWLEDGMENT

This work has received funding from the European Union Horizon 2020 research and innovation programme H2020-MSCA-RISE-2016 under the grant agreement No 734832. The authors are also thankful to Jan Andreas Holm for technical support in designing and assembling the hydraulic setup.

REFERENCES

[1] H. E. Merritt, *Hydraulic control systems.* John Wiley and Sons, 1967.
[2] M. Jelali and A. Kroll, *Hydraulic Servo-systems: Modelling, Identification and Control.* Springer London, 2003.
[3] A. Alleyne and R. Liu, "A simplified approach to force control for electro-hydraulic systems," *Control Engineering Practice*, vol. 8, no. 12, pp. 1347–1356, 2000.
[4] Bin Yao, Fanping Bu, J. Reedy, and G.-C. Chiu, "Adaptive robust motion control of single-rod hydraulic actuators: theory and experiments," *IEEE/ASME Transactions on Mechatronics*, vol. 5, no. 1, pp. 79–91, 2000.
[5] J. Komsta, N. van Oijen, and P. Antoszkiewicz, "Integral sliding mode compensator for load pressure control of die-cushion cylinder drive," *Control Engineering Practice*, vol. 21, no. 5, pp. 708–718, 2013.
[6] G. Liu and S. Daley, "Optimal-tuning nonlinear PID control of hydraulic systems," *Control Engineering Practice*, vol. 8, no. 9, pp. 1045–1053, 2000.
[7] S. S. Tørdal, A. Klausen, and M. K. Bak, "Experimental System Identification and Black Box Modeling of Hydraulic Directional Control Valve," *Modeling, Identification and Control: A Norwegian Research Bulletin*, vol. 36, no. 4, pp. 225–235, 2015.
[8] M. B. Kjelland and M. R. Hansen, "Offshore Wind Payload Transfer Using Flexible Mobile Crane," *Modeling, Identification and Control: A Norwegian Research Bulletin*, vol. 36, no. 1, pp. 1–9, 2015.
[9] M. H. Rudolfsen, T. N. Aune, O. Auklend, L. T. Aarland, and M. Ruderman, "Identification and control design for path tracking of hydraulic loader crane," in *2017 IEEE International Conference on Advanced Intelligent Mechatronics (AIM)*, 2017, pp. 565–570.
[10] B. Eryilmaz and B. H. Wilson, "Unified modeling and analysis of a proportional valve," *Journal of the Franklin Institute*, vol. 343, no. 1, pp. 48–68, 2006.
[11] G. Sohl and J. Bobrow, "Experiments and simulations on the nonlinear control of a hydraulic servosystem," *IEEE Transactions on Control Systems Technology*, vol. 7, no. 2, pp. 238–247, 1999.
[12] H. C. Pedersen and T. O. Andersen, "Pressure Feedback in Fluid Power SystemsActive Damping Explained and Exemplified," *IEEE Transactions on Control Systems Technology*, vol. 26, no. 1, pp. 102–113, 2018.
[13] M. Ruderman, "Full- and reduced-order model of hydraulic cylinder for motion control," in *IECON 2017 - 43rd Annual Conference of the IEEE Industrial Electronics Society*, 2017, pp. 7275–7280.
[14] G. Ferrari-Trecate, M. Muselli, D. Liberati, and M. Morari, "A clustering technique for the identification of piecewise affine systems," *Automatica*, vol. 39, no. 2, pp. 205–217, 2003.
[15] A. L. Juloski, W. P. M. H. Heemels, G. Ferrari-Trecate, R. Vidal, S. Paoletti, and J. H. G. Niessen, "Comparison of Four Procedures for the Identification of Hybrid Systems." Springer, Berlin, 2005, pp. 354–369.
[16] S. Paoletti, A. L. Juloski, G. Ferrari-Trecate, and R. Vidal, "Identification of Hybrid Systems A Tutorial," *European Journal of Control*, vol. 13, no. 2-3, pp. 242–260, 2007.
[17] J.-J. E. Slotine and W. Li, *Applie Nonlinear Control*. Massachusetts: Prentice Hall, 1991.
[18] L. Rodrigues and S. Boyd, "Piecewise-affine state feedback for piecewise-affine slab systems using convex optimization," *Systems & Control Letters*, vol. 54, no. 9, pp. 835–853, 2005.
[19] N. McClamroch and I. Kolmanovsky, "Performance benefits of hybrid control design for linear and nonlinear systems," *Proceedings of the IEEE*, vol. 88, no. 7, pp. 1083–1096, 2000.
[20] Rafal Goebel, Ricardo G. Sanfelice and A. R. Teel, "Hybrid Dynamical Systems," *IEEE Control Systems*, vol. 29, no. 2, pp. 28–93, 2009.
[21] C. Tomlin, I. Mitchell, A. Bayen, and M. Oishi, "Computational techniques for the verification of hybrid systems," *Proceedings of the IEEE*, vol. 91, no. 7, pp. 986–1001, 2003.
[22] Z. Alkhoury, M. Petreczky, and G. Mercère, "Identifiability of affine linear parameter-varying models," *Automatica*, vol. 80, pp. 62–74, 2017.
[23] L. Márton, S. Fodor, and N. Sepehri, "A practical method for friction identification in hydraulic actuators," *Mechatronics*, vol. 21, no. 1, pp. 350–356, 2011.
[24] M. Ruderman, "On break-away forces in actuated motion systems with nonlinear friction," *Mechatronics*, vol. 44, pp. 1–5, 2017.
[25] M. Ruderman and M. Iwasaki, "Observer of Nonlinear Friction Dynamics for Motion Control," *IEEE Transactions on Industrial Electronics*, vol. 62, no. 9, pp. 5941–5949, 2015.
[26] Kramp, "NH 30 cylinder," may 2018.
[27] HBM, "Force Transducers," may 2018.
[28] Moog, "Direct articulated proportional servovalve D633/D634," may 2009.
[29] Danfoss, "MBS 1250, Heavy Duty Pressure sensors," may 2018.
[30] Celesco, "Linear Potentiometer," may 2015.
[31] Speedgoat, "Speedgoat - Rugged Baseline embedded controller for Simulink real-time," apr 2018.